Irradiation-induced amorphization: Effects of temperature, ion mass, cascade size, and dose rate

S. X. Wang,[1] L. M. Wang,[1] and R. C. Ewing[1,2,*]
[1]*Department of Nuclear Engineering & Radiological Sciences, University of Michigan, Ann Arbor, Michigan 48109*
[2]*Department of Materials Science & Engineering, University of Michigan, Ann Arbor, Michigan 48109*
(Received 16 March 2000; published 15 December 2000)

An empirical model based on cascade ''quenching'' and epitaxial recrystallization has been developed to describe the accumulation of the amorphous fraction during ion beam irradiation experiments. The model is based on the assumption that the amorphous fraction that remains after the formation of a cascade is related to a crystallization efficiency parameter *A*. For low values of *A*, as would be expected at low temperatures, for heavy-ion irradiations, or for materials that are good glass formers, the accumulation of the amorphous fraction as a function of dose is an exponential function. For high values of *A*, as would be expected at elevated temperatures, for light-ion irradiations, or for materials that are poor glass formers, the accumulation of the amorphous fraction as a function of dose is a sigmoidal function. Amorphization dose varies as a function of temperature and is reflected by the temperature-dependent crystallization efficiency. The effects of ion mass and energy on critical amorphization dose and temperature are discussed in terms of the cascade size. The dose-rate effect on the critical temperature of amorphization is derived considering the thermal annealing of the damaged material.

DOI: 10.1103/PhysRevB.63.024105 PACS number(s): 61.80.Jh, 64.70.Kb

I. INTRODUCTION

Many materials become amorphous as a result of ion irradiation. Factors that affect ion-beam-induced amorphization include sample temperature, ion mass, ion energy, dose rate, and the properties of the target material. Previous studies have focused on two aspects of radiation-induced amorphization: (1) the susceptibility of a material to amorphization, and (2) the detailed evolution of the crystalline-to-amorphous transition during ion beam irradiation. The first issue has been addressed from different perspectives: thermodynamic stability,[1,2] the topology of the atomic scale structure,[3] physical properties,[4] and ease of glass formation.[5,6] There is a strong correlation between the irradiation-induced amorphization and glass formation.[5,6] This is because radiation-induced amorphization and glass formation are the result of the failure of a material to crystallize from a highly disordered state. The thermodynamic approach has also shown that the enthalpy difference between the amorphous and the crystalline states contributes to the tendency toward the amorphization.[1] Both kinetics and thermodynamics contribute to the amorphization process because together they control the rate of crystallization. Many crystalline substances that have corresponding glasses of the same chemical composition can be readily amorphized by ion irradiation.[6] On the other hand, substances that cannot be amorphized by ion irradiation are generally not found to form glasses.

In this paper, we focus on the second aspect of irradiation-induced amorphization, the detailed process of the crystalline-to-amorphous transition. There are two general approaches used to describe radiation-induced amorphization: the direct-impact model[7,8] and the defect-accumulation model.[7,9,10] The direct-impact model assumes that the amorphous domain forms directly in the core of a displacement cascade in a manner similar to liquid quenching.[7,11–14] Recently, molecular-dynamic simulations have shown that the amorphous region is formed directly from an individual cascade.[15] X-ray diffraction studies on metamict zircon have also suggested that the irradiation-induced amorphization is due to direct-impact damage.[16,17] The defect-accumulation model assumes that the incoming particle produces defects and that the defects accumulate during continued irradiation until an amorphous phase forms when the local defect density reaches a threshold level.[7,9,18,19]

Both the direct-impact and the defect-accumulation models were developed by Gibbons.[7] According to Gibbons, the change in amorphous fraction with ion dose is simply an exponential function for the direct-impact model; while for the defect-accumulation model (or overlap model), the function is sigmoidal. For heavy-ion irradiations, especially at low temperatures, the amorphization process was assumed to be caused by direct amorphization within the cascade. For light ions (or electrons and neutrons), the dominant mechanism was assumed to be by defect accumulation.[7,10,12] Other models have been developed to interpret and to model amorphization induced by ion bombardment.[18,20–26] Most of the recent models are based on defect accumulation or are combined with the direct-impact model.[9,20,24]

Carter's[24] modified Avrami-Johson-Mehl model qualitatively showed that the accumulation of amorphous fraction with increasing ion dose changed from a simple exponential form to a sigmoidal form. However, the parameters affecting the change were not explicitly derived. Carter's model predicts a smaller amorphization dose at higher temperature. This contradicts experimental results (e.g., Ref. 5). In this paper, we present another model in which amorphization is assumed to be the result of direct impact of energetic particles. We also analyze the effects of temperature, dose rate, and ion mass.

II. GENERAL EQUATIONS

The target material is assumed to be a thin foil with a thickness less than the ion range. Each incident ion creates

one or more damaged regions or individual subcascades. When the atoms within an individual damage region share high enough energies (~1 eV), the atoms in the region collectively behave like a ''hot zone.'' [27] The occurrence of such a volume eliminates atomic scale periodicity. By energy dissipation, the ''hot zone'' may be ''quenched'' into an amorphous phase, or partial recrystallization may occur, depending on atomic mobility and the rate of energy dissipation. This process is analogous to glass formation by quenching from a melt. Thus, this process is called ''cascade quenching.'' [5]

The boundary of the cascade may be defined by the temperature contour of the melting temperature. The size of the cascade is the maximum size of the ''melt zone'' because the ''melt zone'' expands and shrinks with the dissipation of energy. A general result of cascade quenching is an amorphous core and a recrystallized shell.[5,6,28] Because of the presence of a crystalline matrix surrounding the cascade, the dominant recrystallization process is epitaxial. We have assumed epitaxial recrystallization is the only crystallization process during cascade quenching in order to simplify the analysis.

The initial equation for the description of the process is based on the lifetime of a single cascade. The formation of the individual cascade with a volume V_0 removes all of the crystallinity within its boundary. During energy dissipation, atomic diffusion (which is radiation enhanced due to the highly energetic state of atoms) causes recrystallization. We use the ''crystallization efficiency'' A to represent the volume fraction of the recrystallized shell within a single cascade, for a crystalline matrix. If there are amorphous ''cores'' left in the displacement cascades, the amorphous fraction will accumulate with the increasing ion dose. Because epitaxial growth relies on a crystalline interface, an increasing amorphous fraction in the material reduces the extent of recrystallization of a cascade. This process is expressed by the following differential equation:

$$\frac{dV_c}{dN} = -mV_0\frac{V_c}{V_T} + AmV_0\frac{V_c}{V_T} + A(1-A)mV_0\left(\frac{V_c}{V_T}\right)^3, \tag{1}$$

where N is the number of ions, m is the number of individual subcascades created by one incident ion, V_T is the total volume of the thin sample (or the damaged layer), V_c is the crystalline volume within V_T, and V_0 is the volume of a subcascade. The first term on the right in Eq. (1) is the crystalline fraction lost due to cascade formation by a single incident ion. The second and the third terms represent the volume that has recrystallized during the quenching process.[13] In the second term, AmV_0 is constant for a specific experiment and V_0/V_T is the fraction of crystalline material in the matrix. Thus, the second term represents recrystallization that is proportional to V_c/V_T. The first two terms give a result that is similar to the direct-impact model of Gibbons.[7] However, the direct-impact model by Gibbons has been found to have limited application.[7,20] Because of this, Gibbons has used a multiple-overlap model (using various overlap times for the cascades).[7] In fact, the assumption of a linear relation of recrystallization to crystalline fraction is arbitrary. This is because the sites for epitaxial growth are directly related to the fraction of the area (rather than volume) that is periodic at the subcascade boundary. The recrystallized volume may develop in any direction from that surface. In this model, we have adopted a simple formulation to describe the recrystallization process: adding a third term to the right-hand side of Eq. (1). This nonlinear term, $\Delta V = A(1-A)mV_0(V_c/V_T)^3$, is formulated based on the analysis that (1) $\Delta V=0$ when $A=0$ (in this case, there is no recrystallization) (2) $\Delta V=0$ when $A=1$ for complete recrystallization (this restriction simply requires that the recrystallized volume not be greater than the subcascade volume), and (3) ΔV is larger for larger V_c/V_T, because the nonlinear term is also controlled by the abundance of crystallization sites. The third term is the nonlinear contribution to the recrystallized fraction that is affected by the geometry and distribution of previously damaged regions; however, the exact value of the exponent is not known. Thus, the exponent is a fitting parameter. Integers (2, 3, 4, and 5) were used in order to obtain a simple solution to Eq. (1). A value of 3 for the exponent provides the best fit to available data.

Integrating the equation from 0 to N ions, and using the initial condition that $V_c/V_T=1$ when $N=0$, the amorphous fraction f_a is

$$f_a = 1-\frac{V_c}{V_T} = 1-\frac{1}{\left[A+(1-A)\exp\left(\frac{mV_0}{V_T}2(1-A)N\right)\right]^{1/2}}. \tag{2}$$

Using D for ion dose (ions/cm^2), the amorphous volume fraction is

$$f_a = 1-\frac{1}{\left[A+(1-A)\exp\left(\frac{mV_0}{h}2(1-A)D\right)\right]^{1/2}}, \tag{3}$$

where h is the sample thickness (assuming h is less than the ion range).

The term mV_0/h is the cross-sectional area of an ion track. We simplify the above equation by combining the term $[D(mV_0/h)]$ into the normalized ion dose D_n. D_n represents the total number of atoms in all damaged regions (or cascades) divided by the total number of atoms in the sample. D_n is similar in form to the definition of displacements per atom (dpa). D_n is proportional to dpa but larger than dpa because we consider all atoms inside a cascade as mobile. As with dpa, D_n is actually an alternative expression of ion dose. Using D_n we have a simple expression for amorphous fraction as a function of ion dose:

$$f_a = 1-\frac{1}{\sqrt{A+(1-A)\exp[2(1-A)D_n]}}. \tag{4}$$

The amorphous fraction as a function of D_n is plotted for different crystallization efficiencies (Fig. 1). For small A, f_a behaves like a simple exponential function. In fact, $f_a=1$

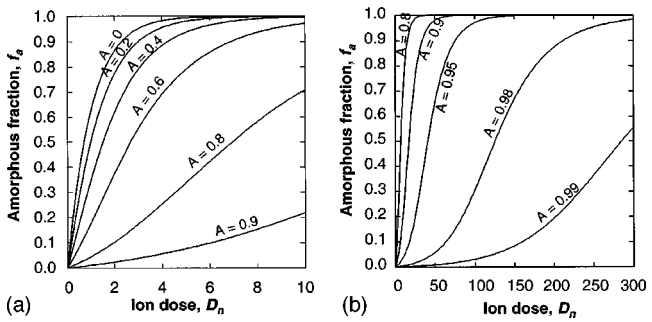

FIG. 1. Amorphous volume fraction f_a as a function of normalized ion dose for different crystallization efficiencies A.

$-\exp(-D_n)$ when $A=0$ in Eq. (4). This is the result of Gibbons's direct-impact model.[7] For large A, especially for A close to 1, the $f_a \sim D_n$ curve is sigmoidal, and the sigmoidal character of the curve becomes more obvious with increasing A. When $A=1$, f_a is zero.

The $f_a \sim D$ curves in Gibbons's overlap model can be closely matched by Eq. (4) using different A values. As will be discussed, the distances between the curves in Fig. 1 reflect the temperature dependence of the amorphization dose.

III. CRYSTALLIZATION EFFICIENCY

Because A represents the extent of recrystallization, it varies with temperature and the properties of target materials. We assume that recrystallization at the cascade-matrix interface is controlled by thermal diffusion under irradiation-enhanced conditions (as assumed by Morehead and Crowder[8] and by Weber, Ewing, and Wang[26]). A diffusion-controlled process is dramatically different from the process of thermal annealing of defects. The recrystallization within a cascade may be considered as ''irradiation-enhanced'' dynamic annealing,[26] due to the uneven distribution of vacancies and interstitials and the high-energy state of the atoms.

As in many thermally controlled processes, such as the defect mobility,[29] annealing of radiation tracks,[30] atomic diffusion,[8] and irradiation-induced amorphization,[24,31] we have assumed that the recrystallization rate R has an Arrhenius form: $R=R_0 \exp(-E_a/kT)$. Thus, the crystallization efficiency A can be written as

$$A=A_0 \exp[-E_a/(kT)], \tag{5}$$

where A_0 is a preexponential constant, E_a is the activation energy for the dynamic annealing of a cascade, k is the Boltzmann constant, and T is the sample temperature.

The preexponential constant A_0 can be determined by specifying a boundary condition. According to Eq. (5), A increases with increasing temperature. When the temperature reaches a certain value, $A=1$ (A is 1 at higher temperatures because that is the maximum extent of recrystallization). At that critical temperature, T_c, the entire damaged region is recrystallized (no further amorphization occurs when $T \geqslant T_c$). We define this temperature as the critical temperature for amorphization, T_c. Using T_c as a boundary condition, Eq. (5) becomes

$$A=\begin{cases} \exp\left[\dfrac{E_a}{k}\left(\dfrac{1}{T_c}-\dfrac{1}{T}\right)\right] & \text{for } T<T_c \\ 1 & \text{for } T \geqslant T_c. \end{cases} \tag{6}$$

Another form of crystallization efficiency, the temperature ratio form, has also been proposed.[13] This form of A is empirical and was formulated based on the idea of a ''liquidlike'' cascade quenching.[13] The general form is

$$A=\begin{cases} 1-\left(\dfrac{T_c-T}{T_m-T}\right)^b & \text{for } T<T_c \\ 1 & \text{for } T \geqslant T_c, \end{cases} \tag{7}$$

where b is a subcascade shape parameter that has a value between 2 and 3, depending on cascade shape ($b=2$ for a cylinder, $b=3$ for a sphere, and $2<b<3$ for an ellipsoid); T_m is the melting temperature; and T_c is the critical temperature of the sample above which full recrystallization occurs.

We use the exponential form of A in our discussion because it is commonly accepted.[8,26] The temperature ratio form of A is used as an alternative because it uses a different set of parameters. The simplicity of the temperature ratio form makes it useful for efficient modeling of experimental data and investigating the effect of cascade size on amorphization.

The crystallization efficiency represented by Eq. (6) includes all of the possible factors that could affect the annealing process, such as temperature. A higher temperature corresponds to a larger A value and more annealing. The activation energy varies for different materials. E_a is a function of atomic bonding and the properties of the cascade. T_c also varies for different materials. Another factor that should affect the critical temperature is the cascade size. Based on a small-volume (such as a cascade) quenching and recrystallization analysis, we obtained an approximate relation of T_c to other parameters:[13]

$$T_c \simeq T_m-(T_m-T_g)R_{\text{cryst}}/(r_0 B), \tag{8}$$

where T_g is the glass-transition temperature, R_{cryst} is the crystallization rate, r_0 is the subcascade radius, and B is a constant related to heat diffusivity. Thus, we may identify general relationships in Eq. (8): (1) for materials that are good glass formers (larger T_g, smaller crystallization rate), T_c is larger; (2) a smaller cascade corresponds to a smaller T_c; and (3) for materials with high crystallization rates, T_c is higher.

IV. APPLICATIONS OF THE MODEL

A. Amorphization accumulation during irradiation

The amorphous fraction accumulation is expressed by Eq. (4) and shown in Figs. 1 and 2. The amorphous fraction accumulation of 360-keV Ar^+ irradiation of α-SiC measured by the Rutherford backscattering spectroscopy technique[32] can be fitted using Eq. (4) (Fig. 3). The curve drawn according to our model, for a crystallization efficiency $A=0.75$, shows a good fit to the experimental data.

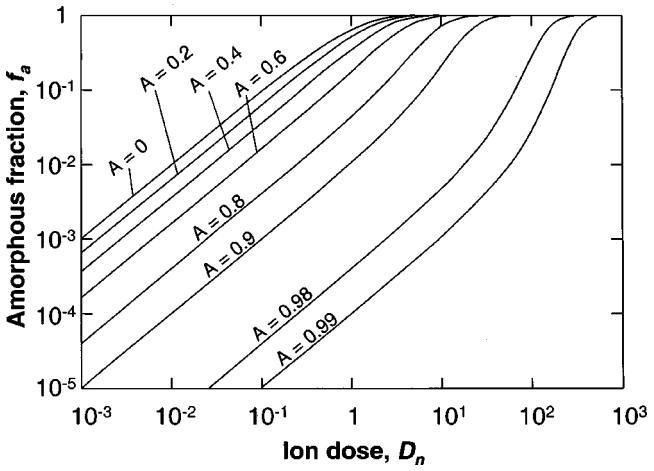

FIG. 2. Double logarithmic scale of f_a as a function of ion dose, showing the gradual change of curve shape as a function of crystallization efficiency A.

In another example, the crystalline fraction of Mylar as a function of ion dose[33] is shown in Fig. 4. The curves are plotted using Eq. (4). The different curves represent the effect of ion mass. The shape of the amorphous accumulation curve changes with ion mass. This is also reflected in the values of A. With decreasing ion mass, A values increase and approach 1 for lighter ions. This ion mass effect is predicted by the model and will be discussed in detail in a following section.

B. Temperature effect

The temperature dependence of the amorphization dose can be easily obtained by solving for D in Eq. (3). We define Δ_c as the detection limit of the crystalline fraction below which the sample is assumed to be ''fully amorphous.'' Δ_c depends on the technique used in measuring the point of ''complete amorphization.'' A value of 1–5 % may be used

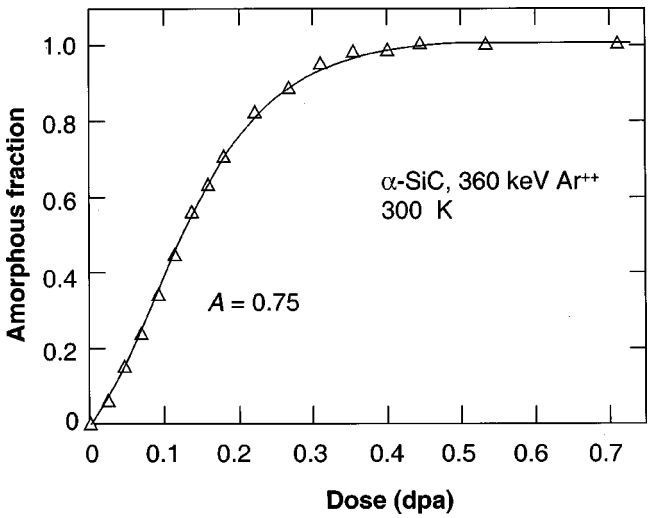

FIG. 3. Relative Si disorder of α-SiC sample irradiated by 360-keV Ar^{2+} at 300 K (Ref. 32). Solid line is fit to the data using Eq. (4).

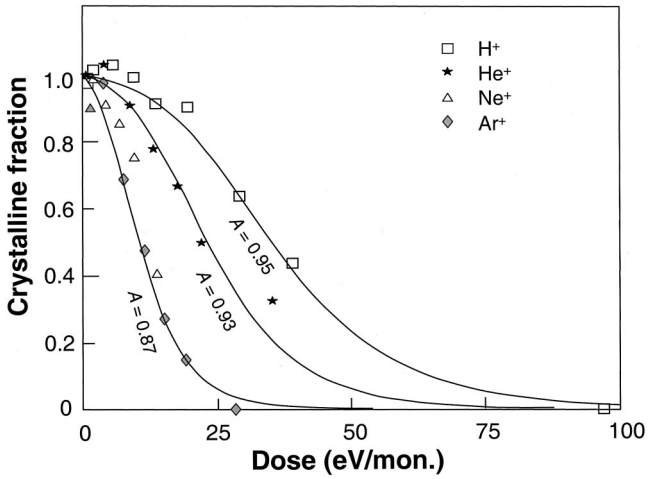

FIG. 4. Crystalline fraction change with ion dose for polymer Mylar irradiated by various ions. Ion dose is in energy fluence, eV monomer. Solid line is fit to the data using Eq. (4).

for most experimental techniques. Replacing $f_c(=1-f_a)$ with Δ_c in Eq. (3) and because $1/\Delta_c^2 \gg A$, the critical amorphization dose is

$$D_c = \frac{h}{2mV_0}\,\frac{\ln(1/\Delta_c^2)-\ln(1-A)}{1-A}. \tag{9}$$

The explicit temperature dependence can be obtained by inserting one of the expressions for A [Eqs. (6) and (7)] into Eq. (9). Thus, we have two expressions for the temperature dependence of amorphization:

$$D_c = \frac{h}{2mV_0}\,\frac{\ln(1/\Delta_c{}^2)-\ln\left\{1-\exp\left[\frac{E_a}{k}\left(\frac{1}{T_c}-\frac{1}{T}\right)\right]\right\}}{1-\exp\left[\frac{E_a}{k}\left(\frac{1}{T_c}-\frac{1}{T}\right)\right]} \tag{10}$$

or

$$D_c = \frac{h}{2mV_0}\,\frac{\ln(1/\Delta_c{}^2)-3\ln\left(\frac{T_c-T}{T_m-T}\right)}{\left(\frac{T_c-T}{T_m-T}\right)^3}. \tag{11}$$

The above equations can be simplified by ignoring the less important terms.[13] The simplified forms of the temperature dependence of amorphization dose are

$$D_c = \frac{D_0}{1-\exp\left[\frac{E_a}{k}\left(\frac{1}{T_c}-\frac{1}{T}\right)\right]} \tag{12}$$

or

$$D_c = \frac{D_0(T_c/T_m)^3}{\left(\frac{T_c-T}{T_m-T}\right)^3}, \tag{13}$$

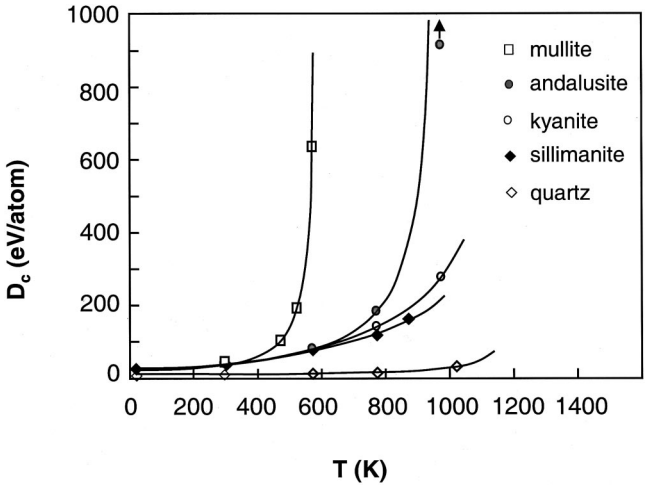

FIG. 5. Temperature dependence of amorphization dose (in energy loss by nuclear collision) of 1.5-MeV Xe^+ irradiation of three Al_2SiO_5 polymorphs, mullite, and quartz (Ref. 5).

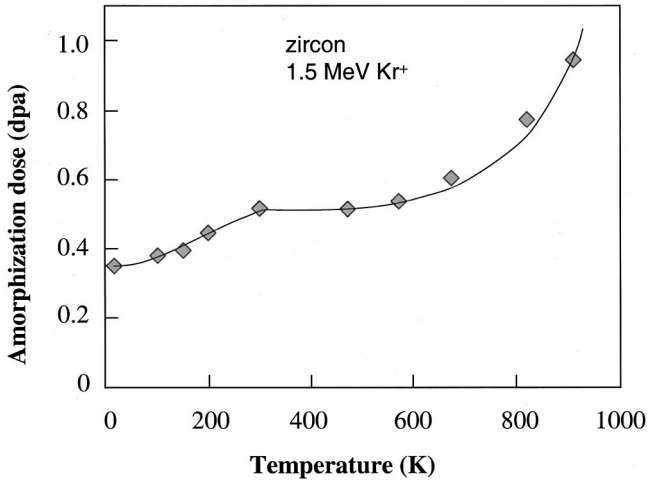

FIG. 6. Temperature dependence of amorphization dose for 1.5-MeV Kr^+ irradiation of zircon (Ref. 26). Solid line is fit to the data using Eq. (14).

where D_0 is the amorphization dose extrapolated to $T=0$ K. D_0 incorporates all the temperature-independent terms (h, m, V_0, and Δ_c). Equation (12) is identical to that derived by Weber, Ewing, and Wang.[26] Numerous experiments[5,13,26] support the temperature dependence of amorphization dose as given by Eq. (12) In Fig. 5, the data of 1.5-MeV Xe^+ irradiation of phases in Al_2O_3-SiO_2 system[5] are compared to the model based on Eq. (12). The activation energies obtained are quartz (0.17 eV), sillimanite (0.041 eV), kyanite (0.038 eV), andalusite (0.036 eV), and mullite (0.028 eV). The value of the activation energy is much smaller than that expected for thermal annealing. For Si, the activation energy for thermally induced epitaxy is 2.35 eV (Ref. 34) and 0.22 eV for epitaxial recrystallization induced by ion irradiation.[35] The meaning and the validity of this activation energy of dynamic annealing during irradiation have been discussed by several authors.[34,36] However, an explicit explanation has not been developed. We may call E_a in Eq. (6) an ''apparent activation energy.'' The small activation energy may be due to the high-energy state and nonequilibrium condition within a cascade.

Many experiments have shown that temperature dependence of critical dose has steps or stages at low temperatures.[26,37,38] Figure 6 is the temperature dependence of amorphization dose of zircon under 1.5-MeV Kr^+ irradiation (data from Weber, Ewing, and Wang[26]), where the step at about 300 K is clearly shown. A reasonable explanation for this phenomenon is that there is significant annealing at relatively low temperatures, and the annealing is complete at the temperature slightly above the step. Weber, Ewing, and Wang attributed the occurrence of the step in the $D\sim T$ curve to the annealing of intracascade defects. To model the steps, we consider the intercascade defects as small-sized cascades. A common picture of cascade formation is that of a larger cascade surrounded by individual displacements or smaller damage regions. We assume that one incident ion creates n large subcascades and m smaller subcascades. We assume that they act independently, each having their own critical temperatures T_{c1} and T_{c2}, and activation energies E_{a1} and E_{a2}. From Eq. (12) we have

$$D_c n = \frac{D_0 n}{1-A_1} \quad \text{for large cascades,}$$

$$D_c m = \frac{D_0 m}{1-A_2} \quad \text{for small cascades.}$$

Combining these two equations, we have

$$D_c = \frac{D_0(m+n)}{m(1-A_1)+n(1-A_2)}, \tag{14}$$

where

$$A_i = \begin{cases} \exp\left[\dfrac{E_{ai}}{k}\left(\dfrac{1}{T_{ci}}-\dfrac{1}{T}\right)\right] & \text{for } T<T_{ci} \\ 1 & \text{for } T\geqslant T_{ci}. \end{cases} \tag{15}$$

Equation (14) features two stages on the $D\sim T$ plot. Depending on the ratio of m/n the step may be obvious or too small to be detected. The two stages are clearly shown in the 1.5-MeV Kr^+ irradiation of zircon (Fig. 6).[26] Using Eq. (14), we can fit the stepwise temperature dependence of the data points. The parameters used in the data fitting are $T_{c1}=300$ K, $E_{a1}=0.02$ eV, $T_{c2}=1120$ K, $E_{a2}=0.31$ eV, and $m/n=2.2$ (one large cascade accompanied with 2.2 small cascades).

C. Ion mass and energy effects

Nuclear stopping power is larger for heavier incident ions. Thus, the subscascade size generally increases with ion mass.[38–40] From the relationship between T_c and subcascade size in Eq. (8), heavier-ion irradiations lead to higher T_c and smaller A. This is clearly shown in Figs. 4 and 7. In Fig. 7(b), the reciprocal of subcascade radius r_0 shows an ap-

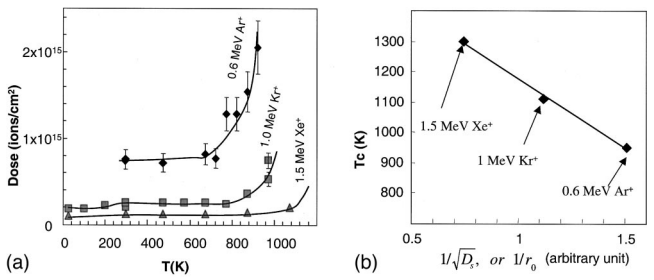

FIG. 7. (a) Temperature dependence of amorphization dose of $Gd_2Ti_2O_7$ irradiated by 1.5-MeV Xe^+, 1-MeV Kr^+, and 0.6-MeV Ar^+ (Ref. 38). (b) The trend of T_c of $Gd_2Ti_2O_7$ changing with the cascade size r_0 for different ions (Ref. 38), where $1/r_0 \sim 1/\sqrt{D_s}$, and D_s is the displacement cross section (which is proportional to the number of displacement events created by one ion, displacements/ion/Å).

proximately linear relation with T_c, as predicted by Eq. (8). The relative subcascade radii are derived from the square roots of the displacement cross sections, which were calculated using TRIM96.[41]

The effect of ion energy is reflected both in subcascade size and activation energy. Ions of higher energy usually have larger ionizing energy losses, which has been shown to enhance annealing. Thus, one possible effect of increasing energy is to decrease E_a. This has the effect of increasing the A value. If the ion energy increases, ion range increases. Individual cascades tend to split into multiple smaller subcascades. This will increase the crystallization efficiency due to the greater surface area between the cascade and crystalline matrix. This analysis is consistent with the observations of 800-keV Kr^+ and 1.5-MeV Kr^+ irradiations of zircon, where lower energy irradiation had a higher T_c (1338 vs 1101 K) and lower amorphization dose (0.43 vs 0.51 dpa at 0 K).[26,42] Thus, in most cases, higher-energy irradiations correspond to a larger value for A. This should lead to higher amorphization dose and a more distinct sigmoidal shape for the $f_a \sim D$ curve. In general, the ion energy effect is small in comparison to ion mass, especially in the high-energy range (>500 keV). This is due to that fact that the subcascade breaks into smaller ones at higher energies so that the individual subcascade size remains roughly constant. Ion energy effects are more complicated than the ion mass effect. The current model cannot provide a relationship of ion energy to T_c, because of the lack of knowledge of the relationship between energy and cascade size. We can only test our model precisely when cascade geometry variations with ion energy are well understood.

D. Dose-rate effects

In above discussion, we have only considered dynamic annealing during the cascade lifetime. If the time interval for forming two cascades in the volume V_0 is long (more time to anneal) or the sample temperature is high (faster annealing), radiation-assisted thermal epitaxial annealing cannot be ignored.[24,34,43] The radiation-assisted epitaxy is due to the abundant points defects produced by ion irradiation.[43] The lifetime of mobile defects can be in the order of one second,[44] which is much longer than that of a displacement cascade. The defects are mobile around the amorphous-crystalline interface and contribute to the epitaxial recrystallization in the time interval of the displacement cascade. This is the model used in the study of radiation-induced epitaxy of crystalline-amorphous interface.[43] Incorporating radiation-assisted epitaxy into our model, we substitute the single crystallization efficiency A with A_1+A_2 in Eq. (4).

$A_1=A_{01}\exp(-E_1/kT)$ is the crystallization efficiency for the dynamic annealing of cascade, and $A_2=A_{02}\tau\exp(-E_2/kT)$ is the crystallization efficiency for radiation-assisted epitaxial annealing. E_1 and E_2 are the activation energies for dynamic annealing and radiation-induced epitaxy annealing, respectively. The time interval of two continuous cascades in the same region is τ. Dynamic annealing A_1 is time independent because it occurs in an approximately fixed time. The defect-assisted annealing, however, is time dependent because its duration is restricted by the time interval between two continuous cascades. τ is the reciprocal of the dose rate J. The complete form of crystallization efficiency is

$$A=A_{01}\exp(-E_1/kT)+A_{02}(1/J)\exp(-E_2/kT). \quad (16)$$

At a critical temperature T_c, $A=1$, thus,

$$1=A_{01}\exp(-E_1/kT_c)+(A_{02}/J)\exp(-E_2/kT_c). \quad (17)$$

Rearranging this equation into

$$A_{02}/J=[\exp(E_2/KT_c)][1-A_{02}\exp(-E_1/kT_c)], \quad (18)$$

we note the first term on the right-hand side of Eq. (18) dominates over the second term with the variation of T_c. If we apply the typical values [for example, $E_1=0.01-0.1$ eV, $E_2=1-10$ eV, and $0<(A_{01}\text{ or }A_{02})<1$], we find the variation of the second term with T_c, in comparison to the first term, is insignificant so that it may be neglected. Thus, to simplify our analysis, we can treat the second part of Eq. (18) as a constant. The relationship of dose rate and T_c is then

$$J=K\exp\left(\frac{-E_2}{kT_c}\right), \quad (19)$$

where K is a constant. This is a well-established relationship in studies of amorphous-crystalline interface movement during irradiation.[31,43,45] Figure 8 shows the dose-rate dependence of critical temperature for Si under various ion irradiations.[45] The linear relationship of $\ln(J)$ and $1/T_c$ exists for all the ions from C to Xe. The increasing T_c from C to Xe also supports the relationship as described in Eq. (8). Equation (19) supports the temperature of zero growth rate of the amorphous-crystalline interface.[43] For a crystalline-amorphous (of same composition) interface, the zero growth rate temperature is found in experiments as a temperature above which the interface grows toward the amorphous region and below which the interface grows toward the crystalline region.[43] This zero growth rate temperature has a similar meaning to T_c, as we have defined in our model.

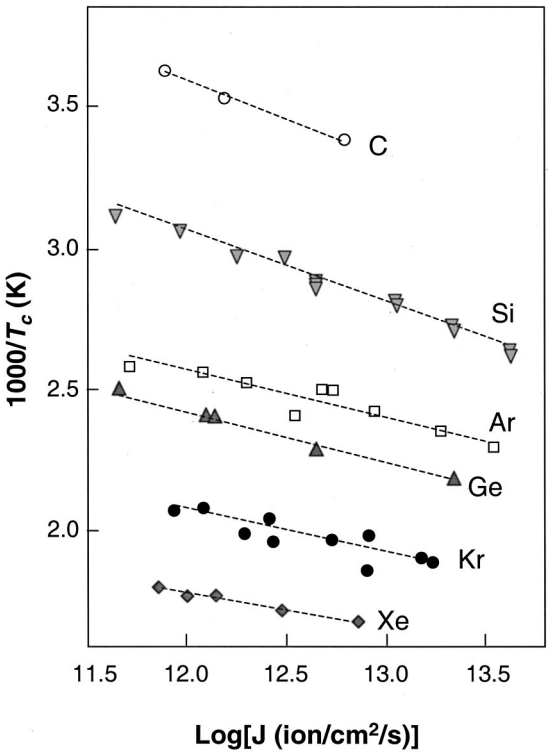

FIG. 8. The dose-rate dependence of critical temperature for Si irradiated with various ions. Data from Goldberg, Williams, and Elliman (Ref. 45).

Equation 19 is also consistent with the observation that a higher dose rate leads to a higher T_c in irradiation-induced amorphization.[40,45] Because the A_2 term is generally smaller than A_1 (due to the larger activation energy of thermal annealing), the equation for amorphized volume accumulation and the temperature dependence of critical dose is generally valid.

E. Materials properties

The different behaviors among materials are captured in their E_a and T_c values. From Eq. (8), T_c decreases with decreasing glass-forming ability (T_g) and decreasing crystallization rate. These are reasonable results if one considers radiation-induced amorphization to be similar to nanoscale glass formation[13] by a quenching process.

Because the activation energy for dynamic annealing is a measure of the energy barrier to atomic movement, it is a function of the target material. Experiments have shown that for a good glass former, the activation energy for dynamic annealing is larger.[5] This is reasonable because it is the larger resistance to atomic movement that makes a good glass former.

In general, materials that are good glass formers have smaller values of A. This should be reflected in a lower amorphization dose and a more exponential-like $f_a \sim D$ curve. On the other hand, materials that are poor glass formers tend to have a larger A. This is reflected in a higher amorphization dose and the more pronounced sigmoidal shape of the $f_a \sim D$ curve.

V. SUMMARY

Based on cascade quenching and the epitaxial recrystallization of a ''liquidlike'' cascade, we have developed a model for irradiation-induced amorphization. For different crystallization efficiencies (the extent of recrystallization), the amorphous fraction accumulation curve changes from a simple exponential to a sigmoidal form. From the temperature dependence of the crystallization efficiency, the temperature dependence of amorphization dose has been derived. Temperature, dose rate, ion mass, cascade size, and the variation of material properties all affect the crystallization efficiency and ultimately the amorphous fraction accumulation.

ACKNOWLEDGMENTS

This work was supported by the Office of Basic Energy Sciences, U.S. Department of Energy under Grant No. DE-FG02-97ER45656.

*Corresponding author. Email address: rodewing@umich.edu

[1] N. Q. Lam and P. R. Okamoto, Mater. Res. Bull. **29**, 41 (1994).
[2] P. R. Okamoto, N. Q. Lam, and L. E. Rehn, Solid State Phys. **52**, 1 (1999).
[3] L. W. Hobbs, Nucl. Instrum. Methods Phys. Res. B **91**, 30 (1994).
[4] R. K. Eby, R. C. Ewing, and R. C. Birtcher, J. Mater. Res. **7**, 3080 (1992).
[5] S. X. Wang, L. M. Wang, R. C. Ewing, and R. H. Doremus, J. Non-Cryst. Solids **238**, 198 (1998).
[6] S. X. Wang, L. M. Wang, R. C. Ewing, and R. H. Doremus, J. Non-Cryst. Solids **238**, 214 (1998).
[7] J. G. Gibbons, Proc. IEEE **60**, 1062 (1972).
[8] F. F. Morehead, Jr. and B. L. Crowder, Radiat. Eff. **6**, 27 (1970).
[9] A. I. Titov and G. Carter, Nucl. Instrum. Methods Phys. Res. B **119**, 491 (1996).
[10] P. Ziemann, W. Miehle, and A. Plewnia, Nucl. Instrum. Methods Phys. Res. B **80/81**, 370 (1993).
[11] H. M. Naguib and R. Kelly, Radiat. Eff. **25**, 1 (1975).
[12] P. Ziemann, Mater. Sci. Eng. **69**, 95 (1985).
[13] S. X. Wang, Ph.D. thesis, University of New Mexico, 1997.
[14] S. X. Wang, L. M. Wang, and R. C. Ewing, in *Microstructure Evolution During Irradiation*, edited by I. M. Robertson, G. S. Was, L. W. Hobbs, and T. Diaz de la Rubia, Mater. Res. Soc. Symp. Proc. No. 439 (Materials Research Society, Pittsburgh, 1997), p. 619.
[15] M. Spaczer, A. Caro, and M. Victoria, Phys. Rev. B **52**, 7171 (1995).
[16] E. K. H. Salje, J. Chrosch, and R. C. Ewing, Am. Mineral. **84**, 1107 (1999).
[17] S. Ríos, E. K. H. Salje, M. Zhang, and R. C. Ewing, J. Phys.: Condens. Matter **12**, 2401 (2000).
[18] J. R. Dennis and E. B. Hale, J. Appl. Phys. **49**, 1119 (1978).

[19] A. T. Motta, L. M. Howe, and P. R. Okamoto, J. Nucl. Mater. **205**, 258 (1993).
[20] W. J. Weber, Nucl. Instrum. Methods Phys. Res. B **166-167**, 98 (2000).
[21] D. A. Thompson, A. Golanski, K. H. Haugen, D. V. Stevanovic, G. Carter, and C. E. Christodoulides, Radiat. Eff. **52**, 69 (1980).
[22] G. Carter, I. V. Katardjiev, and M. J. Nobes, Radiat. Eff. **105**, 211 (1988).
[23] A. Benyagoub and L. Thomé, Phys. Rev. B **38**, 10 205 (1988).
[24] G. Carter, J. Appl. Phys. **79**, 8285 (1996).
[25] A. T. Motta and D. R. Olander, Acta Metall. Mater. **38**, 2175 (1990).
[26] W. J. Weber, R. C. Ewing, and L. M. Wang, J. Mater. Res. **9**, 688 (1994).
[27] J. A. Davies, Mater. Res. Bull. **17**, 26 (1992).
[28] S. X. Wang, L. M. Wang, and R. C. Ewing, in *Microstructural Processes in Irradiated Materials*, edited by S. J. Zinkle, G. Lucas, R. Ewing, and J. Williams, Mater. Res. Soc. Symp. Proc. No. 540 (Materials Research Society, Pittsburgh, 1999), p. 361.
[29] C. R. A. Catlow, Nucl. Instrum. Methods Phys. Res. B **46**, 52 (1990).
[30] H. S. Virk, Nucl. Instrum. Methods Phys. Res. B **65**, 456 (1992).
[31] G. Carter and M. J. Nobes, J. Mater. Res. **6**, 2103 (1991).
[32] W. J. Weber and N. Yu, Nucl. Instrum. Methods Phys. Res. B **127/128**, 191 (1997).
[33] R. M. Papaléo, M. A. de Araújo, and R. P. Livi, Nucl. Instrum. Methods Phys. Res. B **65**, 442 (1992).
[34] J. S. Williams, Mater. Res. Bull. **17**, 47 (1992).
[35] A. La Ferla, S. Cannavó, G. Ferla, S. U. Campisano, E. Rimini, and M. Servidori, Nucl. Instrum. Methods Phys. Res. B **19/20**, 470 (1987).
[36] A. Meldrum, S. J. Zinkle, L. A. Boatner, and R. C. Ewing, Phys. Rev. B **59**, 3981 (1999).
[37] W. J. Weber and L. M. Wang, Nucl. Instrum. Methods Phys. Res. B **91**, 63 (1994).
[38] S. X. Wang, L. M. Wang, R. C. Ewing, G. S. Was, and G. R. Lumpkin, Nucl. Instrum. Methods Phys. Res. B **148**, 704 (1999).
[39] S. Nakao, K. Saitoh, M. Ikeyama, H. Niwa, S. Tanemura, Y. Miyagawa, and S. Miyagawa, Nucl. Instrum. Methods Phys. Res. B **127/128**, 82 (1997).
[40] H. Abe, H. Naramoto, A. Iwase, and C. Kinoshita, Nucl. Instrum. Methods Phys. Res. B **127/128**, 681 (1997).
[41] J. F. Ziegler, J. P. Biersack, and U. Littmark, *The Stopping and Range of Ions in Solids* (Pergamon, New York, 1985).
[42] A. Meldrum, L. A. Boatner, W. J. Weber, and R. C. Ewing, Geochim. Cosmochim. Acta **62**, 2509 (1998).
[43] K. A. Jackson, J. Mater. Res. **3**, 1218 (1988).
[44] M. T. Robinson, J. Nucl. Mater. **216**, 1 (1994).
[45] R. D. Goldberg, J. S. Williams, and R. G. Elliman, Nucl. Instrum. Methods Phys. Res. B **106**, 242 (1995).